Parametric study and multiple correlations on air-side heat transfer and friction characteristics of fin-and-tube heat exchangers with large number of large-diameter tube rows

Gongnan Xie, Qiuwang Wang, Bengt Sunden

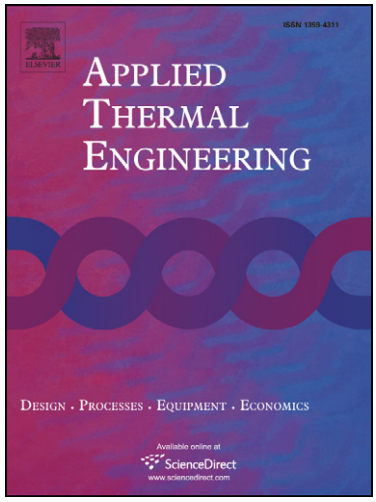

Parametric study and multiple correlations on air-side heat transfer and friction characteristics of fin-and-tube heat exchangers with large number of large-diameter tube rows

Gongnan Xie, Qiuwang Wang, Bengt Sunden

PII: S1359-4311(08)00029-X
DOI: 10.1016/j.applthermaleng.2008.01.014
Reference: ATE 2363

To appear in: *Applied Thermal Engineering*

Received Date: 9 August 2007
Revised Date: 8 January 2008
Accepted Date: 8 January 2008

Please cite this article as: G. Xie, Q. Wang, B. Sunden, Parametric study and multiple correlations on air-side heat transfer and friction characteristics of fin-and-tube heat exchangers with large number of large-diameter tube rows, *Applied Thermal Engineering* (2008), doi: 10.1016/j.applthermaleng.2008.01.014

Revised Manuscript

NOTE: The revised words are marked in blue color.

Parametric study and multiple correlations on air-side heat transfer and friction characteristics of fin-and-tube heat exchangers with large number of large-diameter tube rows

***Gongnan Xie*[a], *Qiuwang Wang*[a],, *Bengt Sunden*[b]**

Gongnan Xie*[a] , *Qiuwang Wang*[a]
[a] State Key Laboratory of Multiphase Flow in Power Engineering,
School of Energy and Power Engineering,
Xi'an Jiaotong University,
Xi'an, 710049, China.
Gongnan.Xie@gmail.com (G.N.Xie)
Corresponding author: wangqw@mail.xjtu.edu.cn (Q.W.Wang)
Tel and Fax: +86-29-82663502

***Bengt Sunden*[b]**

[b]Division of Heat Transfer,
Department of Energy Sciences,
Lund University,
P.O. Box 118, SE-221 00,
Lund, Sweden.
bengt.sunden@vok.lth.se (B.Sunden)
Tel.: +46-46-2228605, fax: +46-46-2224717

Parametric study and multiple correlations on air-side heat transfer and friction characteristics of fin-and-tube heat exchangers with large number of large-diameter tube rows

Abstract

In the present study, for industrial applications of large inter-coolers employed in multi-stage compressor systems the air-side laminar heat transfer and fluid flow characteristics of plain fin-and-tube heat exchangers with large number of tube rows and large diameter of the tubes are investigated numerically through three-dimensional simulations based on the SIMPLE algorithm in Cartesian coordinates. The effects of parameters such as Reynolds number, the number of tube rows, tube diameter, tube pitch and fin pitch are examined, and the variations of heat transfer due to variations of fin materials are also observed. It is found that the heat transfer and fluid flow approach fully developed conditions when the number of tube rows is greater than six, and the tube diameter as well as the fin pitch have much more significant effects than the tube pitch, and the heat transfer of high-conductivity material is larger than that of low-conductivity material especially in the high Reynolds number regime. Due to the fact that the existing correlations are not valid for large tube diameters and number of tube rows, the heat transfer and flow friction of the presented heat exchangers are correlated in the multiple forms. The correlation is so obtained that it can be used for further studies such as performance prediction or geometrical optimization.

Keywords: Plain fin-and-tube heat exchanger; Heat transfer; Friction factor; Parametric study; Multiple correlation

Nomenclature

c_1, c_2, c_3, c_4	Coefficient of formulation
A	Area, m^2
A_f	Fin surface area, m^2
A_{min}	Minimum flow area, m^2
A_o	Total surface area, m^2
c_p	Specific heat at constant pressure, J $kg^{-1}K^{-1}$
D_c	Fin collar outside diameter, $D_c = D_o + 2\delta$, mm
D_i	Inside diameter of tube, mm
D_o	Outside diameter of tube, mm
f	Friction factor
F_p	Fin pitch, mm
h	Heat transfer coefficient, W m^{-2} K^{-1}
M	Number of decision variables
N	Number of tube rows
Nd	Number of sets of data used for correlating
Nu	Nusselt number
ΔP	Pressure drop, Pa
P_l	Longitudinal tube pitch, mm
P_t	Transverse tube pitch, mm
Re	Reynolds number based on D_c
T	Temperature, K
ΔT	Logarithmic mean temperature difference, K
u,v,w	Velocity, m s^{-1}
u_{max}	Maximum velocity at minimum cross-section, m s^{-1}
V_{fr}	Air frontal velocity, m s^{-1}
x,y,z	Coordinates, m

Greek symbols

ρ	Density, kg m^{-3}
λ	Thermal conductivity of fluid, W m^{-1} K^{-1}
λ_f	Thermal conductivity of fin, W m^{-1} K^{-1}
μ	Dynamic viscosity of fluid, kg $m^{-1}s^{-1}$
η_f	Fin efficiency

η	Fin surface efficiency
δ_f	Fin thickness, mm
Φ	Heat transfer rate, W

Subscripts

air	air side
f	fin surface
in	air-side inlet
max	maximum value
out	air-side outlet
p	plain fin
w	tube wall

1. Introduction

To increase thermal performance of heat exchangers, it is necessary and effective to employ extended surfaces (or referred to as finned surfaces) on the gas side to compensate for the low heat transfer coefficient, which maybe 10-to-100 times smaller than that of the liquid-side. Compact Heat Exchangers (CHEs), including two types of heat exchangers such as plate-fin types and fin-and-tube (tube-fin) types, are widely used for gas-gas or gas-liquid applications. CHEs own merits of compactness, small volume, low weight, high effectiveness and low cost. Fin-and-Tube Heat Exchangers (FTHEs) are employed in many power engineering and chemical engineering applications such as compressor intercoolers, air-coolers, fan coils as well as HVAC&R (heating, ventilating, air-conditioning and refrigeration). FTHE (as shown in Fig.1) is one of the successful improvements of the tubular heat exchangers. Because the relatively large thermal resistance, which often accounts to 90% of the overall thermal resistance, is encountered on the gas-side (generally air-side), fins are employed on the gas-side to enlarge the heat exchanger surface area and increase the disturbance of the flow. According to the traditional understanding of the heat transfer enhancement mechanism, an accepted conventional idea adopted in fin surfaces is to disturb the pattern of flow and destroy the boundary layer. Therefore, to satisfy the desire to enhance heat transfer, a variety of plate fin surfaces have been developed and applied successfully.

Although many high-performance fins such as slotted fins, offset strip fins,

louvered fins as well as fins with longitudinal vortex generators have been developed and applied for significant heat transfer enhancements, the corresponding additional pressure drops involved in convective heat transfer are dramatic penalties. For the application where the pressure drop is strictly considered within the specified requirements, the plain fin-and-tube heat exchanger under the design conditions might be a typical type among the choices. At this point, the fin-and-tube heat exchangers having plain fins would not be replaced by those having high-performance fins. Thus, due to the virtues of simple configuration, easy manufacturing, low pressure drop and good reliability, the plain fin-and-tube heat exchangers are still widely used in engineering applications, in which the consumptions of pump or compressor power should be severely managed.

A large number of investigations on the air-side performance for different fin patterns by means of either experimental measures or numerical computations have been carried out. Extensive experimental data or correlations of plain fin-and-tube heat exchangers for refrigeration and air-conditioning applications were established in [1-11]. McQuiston [1] earlier carried out experiments on two samples having the same tube outside diameter of 10.3 mm and fin pitch of 1.78 mm and 3.18 mm, respectively, the test air velocity was ranging between 0.5 m/s and 5.9 m/s. By having tested fourteen samples Rich [2-3] then reported that under the experimental range the intensity of heat transfer did not depend on the fin pitch and the pressure drop per tube was independent of the number of tube rows. McQuiston [4,5] combined the data tested by Rich and his

own data for the same tube diameter of 0.392 in (9.96mm) and fin density of 4, 8, 10, 12 and 14, respectively, and established the widely-known correlations of heat transfer and pressure drop with deviations of $\pm 10\%$ and $\pm 35\%$, respectively. Gray and Webb [6] finally proposed the heat transfer and pressure drop correlations with a square error of 7.3% and 7.8%, respectively. The correlations, having much better precision than that correlated by Rich, are valid for big tubes, large tube pitch and multi-rows. It is emphasized that the correlations were based on the experimental results of four tube-rows and regarded that heat transfer performance was independent of the fin pitch. Kang et al. [7] reported experimental results for nine test samples having the same tube diameter 10.15 mm and fin pitches 2.0 mm, 2.6 mm and 3.2 mm and the number of tube-rows equal to 2, 3 and 4. They provided multiple correlations for all samples within the experimental range. They pointed out that the effect of the fin pitch varies with the Reynolds number and the heat transfer for two tube-rows is better than that for three tube-rows while the heat transfer for three or four tube-rows is similar. Recently, Wang et al. [8-11] stated that for one and two tube-rows the heat transfer is affected by the fin pitch. Having measured the 74 test samples, they established the so-far precise correlation of heat transfer and friction factor having the average deviation of 7.5% and 8.3%, respectively. The correlations have such a wide validation range that they could be applied in the following ranges; tube diameter from 6.35 mm to 12.7 mm, fin pitch from 1.19 mm to 8.7 mm, transverse tube pitch from 17.7 to 31.5 mm, longitudinal tube pitch from 12.4 mm to 27.5 mm as well as the number of tube rows from one to six.

Considerable efforts on numerical studies of plain fin-and-tube heat exchangers were reported in [12-17]. Bestani et al. [18] earlier conducted three-dimensional simulations on pattern of flow passing around a cylinder. Torikoshi and Xi [13] simulated the heat transfer and fluid flow for one and two tube-rows plain fins, in which they found the existing problem. They also compared results obtained from two-dimensional and three-dimensional computations and found difficulties in the three-dimensional simulations. Jang et al. [14] reported that the heat transfer is independent of the number of tube-rows when this number is larger than four, and the heat transfer coefficient and friction factor of staggered tube arrangement offers 15% to 27%, and 20% to 25%, respectively, higher than those of in-line tube arrangement. Jang and Yang [15] conducted numerical computations and experimental measurements of plain fin-and-tube heat exchangers having round tubes and flat tubes, respectively. They found that for the same perimeter of the tubes, the heat transfer coefficient for the flat tube heat exchanger was 35% to 50% higher than that for the round tube heat exchanger while the pressure drop of the former is 25% to 30% of that of the latter. He et al. [16] computed laminar heat transfer of plain fin-and-tube heat exchangers with the number of tube rows from one to three, based on the SIMPLER algorithm in body-fitted coordinates. From the field synergy principle point of view, they analyzed the mechanism of heat transfer enhancement for describing their numerical results. Erek et al. [17] used CFD to study the effects of geometrical parameters on performance of plain fin-and-tube heat exchangers with flat tubes, and they suggested that the increase

of ellipticity could increase the heat transfer together with a distinct decrease of the pressure drop.

From the foregoing reviews of recent findings, one can examine that most of the studies focused only on small numbers of tube rows (mostly less than 4) or small tube diameter (mostly in the range of 8 to 13 mm), which are usually used in the HVAC&R engineering. However, only a small quantity of efforts has focused on large number of tube rows and large tube diameter. In some certain applications of large industry, such as the intercooler of multi-stage compressor, the number of tube rows (might be larger than 4 or much larger) and the outside diameter of tubes is large (might be larger than 13 mm or much larger)**.** The industrial background of the present study is that heat exchangers are applied and operating as inter-coolers in multi-stage compressors to decrease the outlet temperature of compressors and the power input for the compression. This results in improved compressor efficiency and hence improved global efficiency of high pressure thermal plants like as gas turbine plants. Such a kind of heat exchanger is operated under a large heat duty associated with large heat transfer area that might be achieved by a large number of large-diameter tube rows (6 to 12 or higher), because more fins are arranged in the line along the flow direction while a heat exchanger with few tube rows in the flow direction sometimes cannot satisfy the real requirement. Furthermore, at such conditions of gas turbine plants, the consideration of pressure losses in the compressor systems will be very important. Therefore, it is essential to investigate the heat transfer and friction characteristics of fin-and-tube heat exchangers

with large number of tube rows and large tube-diameter (Xie [18], Tang et al. [19,20]). On the other hand, for the presented fin-and-tube heat exchanger having large number of tube-rows and large tube diameter it might not be possible to find suitable correlations for prediction of heat transfer and fluid flow even if there are many existing precise correlations that can be borrowed. So based on the numerical computations of the present study the heat transfer and friction factor should be correlated in certain assumed forms and in turn these correlations could be used for further studies such as design optimizations [21,24] and performance predictions [25,26].The above-mentioned reasons indicate that the results of the present study should be used as a reference**.** For this reason, the objectives of this study are to examine the effects of geometrical parameters on laminar heat transfer of plain fin-and-tube heat exchangers and to correlate the performance in multiple forms based on the numerical results.

In the following sections, the problem and physical model investigated are first described in Section 2, and the reasons for the selection of flow model and computational domain are included. Having introduced the computational model, the governing equations and boundary conditions are then specified, and the numerical method is also briefly described in Section 3. The experimental sample tested by Kang et al. [7] is then numerically computed and the corresponding numerical results are compared with the experimental results as well as those by Wang et al. [8-11]. This is so to verify the reliability of the assumed model and code developed in this study as well as the grid independence. All these matters are provided in Section 4. The effects of six

parameters are examined in Section 5, where also results and discussion are included. Based on the numerical results in the previous sections, multiple correlations are obtained in Section 6. The conclusions are drawn in the final section.

2. Physical model and assumptions

2.1 Physical model

A schematic diagram of a plain fin-and-tube heat exchanger is shown in Figure 2. It is noted that for saving space and to provide a clear description, the core of a fin-and-tube heat exchanger having three tube-rows is only schematically pictured (however, the effects of the number of tube-rows from two to seven are examined). In fact, in most practical manufacturing, the heat exchanger cores with large tube-rows are often combined from cores with three tube-rows. The fact is that the samples with six or nine tube-rows manufactured in our Laboratory are indeed created from cores having three tube-rows. As shown in Fig. 2(a), hot air flows across a finned tube bundle while cold water flows inside the round tubes that are arranged staggered. The heat is transmitted to the air through the tube wall and fin surfaces, resulting in cooling of the water. The heat transfer and pressure drop characteristics on the air side are to be found by numerical computations based on the suggested model. There are many parameters to describe the configuration of the heat exchanger. Among these parameters the main geometrical parameters are tube outside diameter (D_o), fin pitch (F_p), tube transverse pitch (P_t) and tube longitudinal pitch (P_l). Their nominal values are 18 mm, 3 mm, 42

mm and 34 mm, respectively. The tubes and fins are made of copper (later the effect of material is also observed). The fluid is assumed to be incompressible with constant properties, and the flow is steady state. Due to the relatively large heat transfer coefficient between the cooling water and the inner wall of the tube and the large thermal conductivity of the tube wall, the tube is assumed to be at constant temperature. However, the temperature distribution in the fin surface has to be calculated. Therefore, the computations are of conjugated type, in which both the temperature in the solid fin surface and in the fluid are to be determined simultaneously [27].

2.2 Adoption of flow model

Prior to conducting the numerical computations, discussion is now focused on the adoption of flow regime for the computational model, i.e., laminar or turbulent. The choice of flow model should be motivated in some way as the flow is complex inside compact heat exchanger passage and sufficient experimental data is not available for judgement**.** In this study a laminar flow model is adopted in all computations with the Reynolds number being varied from 1000 to 6000 (based on fin collar outside diameter, $D_c = D_o + 2\delta_f$), the corresponding air frontal velocity is ranged from 0.67 m/s to 4 m/s. The basic considerations are as follows. First, if the flow between two adjacent fin surfaces is regarded as a flow between parallel plates, i.e., a channel flow, the transition Reynolds number may take a value around 2300 using twice the space/pitch between the plates as the reference length. It should be noted that in this study the tube diameter is six times larger than the fin pitch (18 mm and 3 mm, respectively). Thus the

value of Reynolds number of 2300 corresponds to around 6900 based on the fin collar outside tube diameter as reference length in the Reynolds number estimation. The flow may become turbulent when the Reynolds number exceeds 7000. Also, if the flow between two adjacent fin surfaces, where the tube-obstacle is inserted, is considered as a flow past a cylinder, textbooks in fluid mechanics show that turbulent flow occurs at Reynolds numbers larger than 1.4×10^5 based on the diameter of the cylinder. Thus the calculated Reynolds number in the present study is also less than this value. In addition, several studies including laminar heat transfer using similar computational models have been published in international journals [14-16, 28-32]. This gives support and justification that a laminar flow model might be acceptable in the computations**.**

2.3 Computational domain

Having selected the laminar model for computations, the computational domain then has to be clearly specified. Based on the geometrical configuration of symmetry and periodicity, the cell between two adjacent fin surfaces is simulated, i.e., the fin surfaces include half of the fin thickness at the upper and bottom sides while the air flows inside a channel set up by the two solid-fluid interfaces and the obstructing tubes. The computational domain is schematically shown in Fig. 2 (d). In this figure, x refers to the stream-wise coordinate, y denotes the span-wise coordinate, and z stands for the fin pitch direction. Because of the thickness of the fin, the air velocity profile at the entrance is not uniform. The computational domain is then extended upstream 1.5 times the stream-wise fin length so that a uniform velocity distribution can be ensured at the

domain inlet. Similarly, the computational domain is extended downstream 5 times the stream-wise fin length, so the one-way coordinate assumption can be adopted at the domain outlet [27]. Thus the whole stream-wise length of the computational domain is 7.5 times of the actual fin length. To save space, the extended domain is not presented at scale in Fig. 2. In the next section the governing equations as well as the boundary conditions and the numerical method for the computations are explained.

3. Mathematical formulation and numerical method

3.1 Governing equations and boundary conditions

Based on the foregoing assumptions, the numerical computation is based on that the fluid is incompressible, its properties are constant and the flow is steady-state laminar. The governing equations for continuity, momentum and energy in the computational domain may be expressed in tensor form as follows.

Continuity equation

$$\frac{\partial u_i}{\partial x_i} = 0 \tag{1}.$$

Momentum equations

$$\frac{\partial}{\partial x_i}(u_i u_k) = \frac{\mu}{\rho}\frac{\partial}{\partial x_i}(\frac{\partial u_k}{\partial x_i}) - \frac{1}{\rho}\frac{\partial p}{\partial x_k} \tag{2}.$$

Energy equation

$$\frac{\partial}{\partial x_i}(u_i T) = \frac{k}{\rho c_p}\frac{\partial}{\partial x_i}(\frac{\partial T}{\partial x_i}) \tag{3}.$$

The governing equations are elliptic that boundary conditions are specified for all boundaries of the computational domain. Because of the conjugated type of the problem,

the fin surfaces are considered as part of the solution domain and are treated as a special type of fluid. Similar treatments can be found in references [16,28-32]. Necessary conditions must be assigned for the three regions as follows.

(1) At the upstream extended region (domain inlet)

At the inlet:

$$u = const, \quad T = const, \quad v = w = 0 \tag{4}.$$

At the upper and lower boundaries:

$$\frac{\partial u}{\partial z} = \frac{\partial v}{\partial z} = 0, \qquad w = 0, \qquad \frac{\partial T}{\partial z} = 0 \tag{5}.$$

At the front and back sides:

$$\frac{\partial u}{\partial y} = \frac{\partial w}{\partial y} = 0, \qquad v = 0, \qquad \frac{\partial T}{\partial y} = 0 \tag{6}.$$

(2) At the downstream extended region (domain outlet)

At the upper and lower boundaries:

$$\frac{\partial u}{\partial z} = \frac{\partial v}{\partial z} = 0, \qquad w = 0, \qquad \frac{\partial T}{\partial z} = 0 \tag{7}.$$

At the front and back sides:

$$\frac{\partial u}{\partial y} = \frac{\partial w}{\partial y} = 0, \qquad v = 0, \qquad \frac{\partial T}{\partial y} = 0 \tag{8}.$$

At the outlet boundary:

$$\frac{\partial u}{\partial x} = \frac{\partial v}{\partial x} = \frac{\partial w}{\partial x} = \frac{\partial T}{\partial x} = 0 \tag{9}.$$

(3) At the regions of the plain fins

At the upper and lower boundaries:

$$u = v = w = 0, \qquad \frac{\partial T}{\partial z} = 0 \tag{10}.$$

At the front and back sides:

$$\text{fluid region} \quad \frac{\partial u}{\partial y} = \frac{\partial w}{\partial y} = 0, \qquad v = 0, \qquad \frac{\partial T}{\partial y} = 0 \tag{11a}$$

$$\text{fin surface region} \quad u = v = w = 0, \qquad \frac{\partial T}{\partial y} = 0 \tag{11b}$$

$$\text{tube region} \quad u = v = w = 0, \qquad T_w = const \tag{11c}$$

3.2 Numerical method

It is obvious that the problem studied is a fluid-solid conjugated heat transfer problem, which may be solved by the full-field computational method. The solid (herein referring to fins and tubes) in the computational domain is considered as a special fluid with infinite viscosity. The harmonic mean method is adopted for the interface diffusion coefficient. In order to guarantee the continuity of the flux rate at the interface, the thermal conductivity of the fin and fluid adopt individual values, while the heat capacity of the solid is set to be the value of the fluid. A special array is introduced to identify different regions: fluid, fin, and tube. The circular shape of the tube is approximated by the step-wise method. A very large value of the thermal conductivity is assigned to the tube region to ensure the tube temperature to be constant. The detailed computational method of conjugated heat transfer can be found in [27] and similar treatments of different regions can be found in [28-32]. The computational domain is discretized by nonuniform grids with the grids in the central fin region being very fine while those in the extension domains being coarse (as partly shown in Fig. 3). Governing equations are discretized by means of the finite-volume method, and the convection term is

discretized by adopting the power-law scheme [27]. The coupling between pressure and velocity is conducted by the SIMPLE algorithm [33]. Based on the very recent experiences and suggestions [31,32], the convergence criterion for the velocities is that the maximum mass residual of the cells divided by the inlet mass flux is less than 6.0×10^{-7}, and the criterion for temperature is that the difference between two heat transfer rates obtained from an iteration and after 50 successive iterations is less than 1.0×10^{-7}.

3.3 Parameter definition

To improve the physical understanding, some characteristic and non-dimensional parameters are introduced.

$$Re = \frac{\rho u_{\max} D_c}{\mu} \tag{12}.$$

$$\eta h = \frac{\Phi}{A\Delta T} \tag{13}.$$

$$\Phi_h = mc_p(T_{\text{out}} - T_{\text{in}}) \tag{14}.$$

$$Nu = \frac{hD_c}{\lambda} \tag{15}.$$

$$\Delta T = \frac{T_{\max} - T_{\min}}{\ln(T_{\max}/T_{\min})} \tag{16}.$$

$$\Delta p = p_{in} - p_{out} \tag{17}.$$

$$f = \frac{\Delta p}{\frac{1}{2}\rho u_m^2}\frac{D_c}{L} \tag{18}.$$

Here u_{max} is the maximum velocity at the minimum free flow cross-section, T_{in} and T_{out}

are the bulk temperatures at the inlet and outlet section of the fin surface, respectively, and $T_{\max} = \max(T_{in} - T_w, T_{out} - T_w)$, $T_{\min} = \min(T_{in} - T_w, T_{out} - T_w)$. P_{in} and P_{out} are the bulk pressures at inlet and outlet section of the fin surface**,** respectively.

The surface efficiency, η, is defined as the actual heat transfer rate for the fin and base divided by the heat transfer rate for the fin and base when the fin is at the same base temperature T_w. This term may be written in terms of the fin efficiency η_f, fin surface area A_f and total surface area A, i.e.,

$$\eta = 1 - \frac{A_f}{A}(1 - \eta_f) \tag{19}$$

where $A = A_f + A_b$, A_f and A_b are the areas of the fin and base surface, respectively. η_f denotes the fin efficiency and is calculated by the approximation method described by Schmidt [34]

$$\eta = \frac{\tanh(mr_c\phi)}{mr_c\phi} \tag{20}$$

where

$$m = \sqrt{\frac{2h_o}{\lambda_f \delta_f}} \tag{21}$$

$$\phi = (\frac{R_{eq}}{r_c} - 1)[1 + 0.35\log_e(\frac{R_{eq}}{r_c})] \tag{22}$$

$$\frac{R_{eq}}{r_c} = 1.27\frac{X_M}{r_c}(\frac{X_L}{X_M} - 0.3)^{0.5} \tag{23}$$

$$X_L = \sqrt{(P_t/2)^2 + P_l^2}/2 \tag{24}$$

$$X_M = P_t/2 \tag{25}$$

4. Validation of the model and grid independence

4.1 Grid independence

Before examining the effects of geometrical parameters on the performance of heat transfer and flow friction, it is necessary to adopt an appropriate grid system for computations in turn leading to a correct physical understanding. Thus a grid refinement study was conducted to investigate the influence of the grid density on the computational results. Four sets of grid system, 161-42-22, 161-42-32, 201-62-22 and 201-62-32 were selected to check the grid independence, and the computations are performed for a case with Reynolds number being 3000. The results of the four sets of grid system are shown in Fig. 4. By examining the results, the difference between 161-42-22, 161-42-32 and 201-62-22 is not so evident. Through the test experience for the present model, it is found that the finer grid system will result in slightly smaller Nusselt number and friction factor. Comparing the results on the finest grid 201-62-32 with those of the grid 201-62-22 yields 1.2% higher Nusselt number (being 25.86 and 25.39, respectively). Thus to save computer resources and keeping a balance between computational economics and accuracy, the grid system 201-62-22 is adopted in all computations. These are performed on a PC with a CPU frequency of 2.8G and a core memory of 1G. A typical running time for computation of a case is about one to two days, and all of cases composing 46 different tests will last more than three months.

4.2 Validation of the computational model and code

Prior to conducting the computations for examination, it is very necessary to

validate the computational model and the code developed in this study. Preliminary computations were first conducted for a plain fin-and-tube heat exchanger having two tube-rows, for which measurements had been performed by Kang et al. [7]. The geometrical configuration is schematically shown in Fig. 5 (a). The predicted pressure drop and Nusselt number were compared with the corresponding correlations as well as experimental correlations established by Wang et al. [8-11] as shown in Fig. 5 (b). It has to be recalled that the correlations developed by Wang et al. were developed based on 74 samples of plain fins and could describe 85.1% of the database for pressure drop and 88.6% of the database for heat transfer [9]. From the Fig. 5(b), the maximum deviation in pressure drop and the Nusselt number are less than 15% with the average deviation being around 8%. The good agreement between the predicted and tested results shows the reliability of the physical model and the developed code.

An additional comparison between the present numerical results and correlations by Wang's group [18-20, 35] was made, as shown in Fig.6. It should be noted that Tang et al. [19-20] conducted experiments in the Reynolds number range from 4,000 to 10,000 because of restrictions of the wind tunnel capacity. Tang et al. [35] used the commercial software FLUENT to compute turbulent heat transfer of the configuration at Reynolds numbers being 4,000 to 8,000 flow status might be regarded as transition or turbulent flow. The correlations by Gray and Webb [6] might predict the performance of heat exchangers having large-diameter tubes, but the number of tube rows are restricted to four. From the figure, the average deviation of the *j*-factors is around 10% while the

average deviation of the *f*-factors is around 20% in the computational *Re* range. It may not be reliable to extend the correlations developed in the experimental Re range are extended to the low Re region where the laminar flow may occur. As one expects, the heat transfer *j*-factor of the present computations is lower than that of the correlation while the friction factor of the former is higher than that of the latter in the experimental range.

As discussed in Section 2.2, a laminar flow model might be acceptable in the computations. Thus from the above two comparisons, the presented model for computations of laminar flow is validated for the specified Reynolds numbers of 1,000 to 6,000 in this study (Re_{Dh}=250~800, u=0.5~4 m/s). Similar validation can be found in [28-32]. It is concluded that the desire to fill the data in low Reynolds number regions, the laminar model for computations is accurate enough to predict the heat transfer and friction characteristics of such heat exchangers in the industry applications with the inlet frontal velocity usually being in the range of 2 to 4 m/s.

5. Numerical results and discussion

5.1 The effect of number of tube rows

First the effect of the number of tube rows on laminar heat transfer are examined based on the nominal sizes: D_o=18 mm, P_t=42 mm, P_l=34 mm, fin pitch=3 mm, while the number of tube rows being varied from two to seven (N=2~7). The numerical results of Nusselt number and friction factor with different number of tube-rows are

shown in Fig. 7. The characteristics may be summarized as follows. Firstly, it is clear for understanding that with the increase of Reynolds number the Nusselt number *Nu* increases (hence the higher heat transfer) while the friction factor *f* decreases. Secondly, one can carefully examine that the Nusselt number and friction factor are almost identical to those of a heat exchanger with the number of tube rows being six when the number of tube rows being larger than six. That is to say, the heat transfer and pressure drop characteristics are independent upon the number of tube rows when this value is larger than six, after which the heat transfer and fluid flow approach the fully developed state. Thus for the present computational model, there is no need to compute the laminar heat transfer when *N*>=8.

Figure 8 presents the local distributions of the streamlines for the middle section in the x-y plane at z=0.015 between the upper and lower sides of the fin for *Re*=3000 and *N*=2,7. For clearity reasons, the last three-rows distribution of N=7 is presented. It can be clearly seen from the figure that there are larger recirculation zones behind each tube of N=7 than those of N=2. It is recognized from fluid mechanics that a dead flow zone is characterized by a stationary recirculation region that formed in such conditions that the flow separates at the rear portion of a tube and reattaches ar the front of the following tube. The dead flow zone will deteriorate the convective heat transfer. This can be analyzed by Figure 9. Comparing the isotherms of N=2 and N=7, bigger temperature gradients around tubes exist for the N=2, indicating a larger heat flux between the tubes and fluid resulting in large local heat transfer and hence global heat

transfer. This is reflected in the Nusselt number (hence the heat transfer coefficient), which is larger for N=2 than for N=7. Another feature can be clearly seen in Fig. 9. The convective heat transfer coefficient for N=7 approaches the fully developed state which is characterized by a marked periodic temperature level while for N=2 the heat transfer occurs in the inlet region.

5.2 The effect of tube diameter

Having examined the effects of the number of tube rows, it will be expected that under different the number of tube rows the trends of effects of other parameters, e.g., fin pitch, tube diameter and tube pitch, might be similar. Thus for saving the computational resources and the main objective is to observe the effects of fin pitch, tube diameter and tube pitch, the computations are conducted under number of tube rows of three and the Reynolds number *Re* of 3000. Figure 10 shows the effect of the tube diameter on laminar heat transfer. The tube diameter is varied from 16 mm to 20 mm. It can be seen that both the Nusselt number *Nu* and friction factor *f* increase with increasing tube diameter. However, it will not indicate that both the heat transfer and the pressure drop increase with the increase of tube diameter. Actually the heat transfer coefficient decreases with increasing tube diameter. This is because that by keeping the same Reynolds number at the definition of $Re = \rho u_{\max} D_c / \mu$, the increase of tube diameter means a decrease in velocity, which results in decreases of the heat transfer coefficient and pressure drop. The isotherms on similar position for D=16 mm and D=20 mm are displayed in Figure 11. It can be clearly seen from the marked

temperature level that there are bigger temperature gradients around tubes of D=20 mm than those of D=16 mm, indicating that a larger local heat flux, and hence global heat transfer, occurs for D=20 mm. It can also be seen that the temperature gradient along the longitudinal flow direction for D=20 mm is much larger than that of D=16 mm. Consequently it can be concluded that for a fixed Reynolds number the heat transfer enhancement may be increased by increasing the diameter of the tubes employed in finned-tube heat exchangers. In contrast, for a fixed inlet frontal velocity the heat transfer can be improved by decreasing the tube diameter.

The idea to use smaller-diameter tubes in Refrigeration Engineering for heat transfer enhancement is witnessed from this point. But for the present heat exchanger which is applied for large inter-coolers with the cooling media being water, the decrease of tube diameter will lead to decrease of heat transfer under the same water velocity inside the tubes, while under the same mass flow rate the decrease of tube diameter will lead to an increase of water velocity, resulting in larger pressure drop inside the tube. According to the background of large inter-coolers, the heat transfer and pressure drop should be considered at a balance for design and operation. Thus it is an essential issue of investigating the heat exchanger with both tube diameter and the number of tube rows being large, which fortunately is addressed in this study.

5.3 The effect of fin pitch

The effect of fin pitch on laminar heat transfer is shown in Fig. 12. The number of tube rows is three and the Reynolds number is 3000. The fin pitch is ranging from 1.5

mm to 4.5 mm. From the figure, it can be clearly seen that with the increase of fin pitch the Nusselt number *Nu* and friction factor *f* decrease. That is, both the heat transfer and pressure drop increase with the decrease of fin pitch. The decrease of fin pitch means the decrease of space of channel width, resulting in higher velocity and temperature gradient at the fin wall, hence the higher pressure drop and heat transfer. Figure 13 presents the isotherms at similar positions for F_p=2 mm and F_p =4 mm. It also can be clearly seen from the marked temperature level that the temperature gradients around the tubes and along the flow direction of F_p=2 mm are larger than those of F_p=4 mm. This feature can be interpreted so that a smaller fin pitch results in larger heat transfer. It is a fact that for the fixed volume of the heat exchanger the compactness will increase as the fin pitch decreases, since in this way more fins will be stacked together resulting in enlargement of the extended fin surface area. So the pursuit of adding area will lead to heat exchanger being more compact. At this point, by the use of narrow channel the enhancement of heat transfer might be fulfilled.

5.4 The effect of tube pitch

Figure 14 shows the effect of the tube pitch on laminar heat transfer. The number of tube rows is three and the Reynolds number *Re* is fixed at 3000. The longitudinal pitch is varied from 32 mm to 36 mm and the transverse pitch is varied from 19 mm to 23 mm (because of the symmetrical domain, the real transverse pitch is varied from 38 mm to 46 mm). Two features can be noted as follows. Firstly, it is found that for the same air maximum velocity at minimum free flow cross-section, u_{max}, the overall

Nusselt number decreases with the increase of the tube pitch, shown in Fig.14(a) and Fig.14(b). However, it is not stated that the heat transfer is decreased by increasing the tube pitch under the fixing the Reynolds number. In fact, as shown in Fig.14(c) and Fig.14(d), the heat transfer rate increases with the increase of tube pitch. Since the Reynolds number and hence the maximum velocity is fixed, an increased of span-wise/transverse tube pitch means an increased inlet/oncoming flow velocity hence an improved heat transfer. Saying on the contrary way, if the oncoming flow velocity is fixed the maximum velocity will be decreased by increasing the tube pitch, thus with a fixed oncoming flow velocity the increase of tube pitches will lead to an decrease of heat transfer. Similar trends can be found in previous works by He et al. [16]. Secondly, by comparing carefully on heat transfer rate, the effect of transverse pitch is more pronounced than that of the longitudinal pitch. However, for the test ranges of the tube pitches, the effects are relatively smaller than those of the tube diameter and fin pitch.

5.5 The effect of material of fin

The above numerical results are based on copper as the fin material. In some certain applications, e.g., HVAC&R engineering, fin surfaces are widely made in aluminum. In this study the effect will be observed by the numerical computations. The results of the fin surface material in copper (labeled by *Cu*-fin) and aluminum (labeled by *Al*-fin) are shown in Figure 15. The number of tube rows is seven while other geometrical parameters are kept at nominal values. The individual feature for each

sub-figure can be stated as follows. In Fig. 15(a), the Nusselt number of the *Cu*-fin is smaller than that of the *Al*-fin. This will not indicate that the heat transfer of *Al*-fin is higher than that of *Cu*-fin. Recall that in Eq. (13) and Eq. (15) the heat transfer coefficient is separated from the total heat transfer coefficient (although in some countries like Japan or Korea the heat transfer coefficient includes the fin surface efficiency). The total heat transfer coefficients, including the fin surface efficiency, are shown in Fig. 15 (b). It can be clearly seen that the Nusselt number of the *Cu*-fin is much higher than that of the *Al*-fin. Without further thinking one might get the impression that the features from Fig. 15(a) and Fig. 15(b) seem inconsistent. In this situation, a further analysis should clarify this. Going back to Eq. (20) and Eq. (21), the increase of the fin thermal conductivity will lead to a decrease of *mH*, resulting in an increase of the fin efficiency due to the characteristics of the tangent function. The thermal conductivity of the *Cu*-fin is 398 W/(m.K) while that of the *Al*-fin is 170 W/(m.K). Obviously, for the same conditions the efficiency of the *Cu*-fin is surely larger than that of the *Al*-fin. This feature is confirmed in Fig. 15(c). Another traditional feature is that the fin efficiency decreases as the Reynolds number is increasing. The heat transfer rate for the two kinds of fins are compared in Fig. 15(d). By examining carefully, it is found that the heat transfer rate of the *Cu*-fin is higher than that of the Al-fin. Therefore a somewhat important conclusion is that the heat transfer performance of the fin surface will be enhanced especially at high air velocities, since higher thermal conductivity of the fin surface will lead to a smaller thermal resistance.

6. Multiple correlations

6.1 The assumed form of correlations

Based on the above series of parametric computations, it is not sufficient to end up only with the numerical results, but the data of heat transfer and flow friction should be compressed in compact form so that further studies are enabled. This is a common way to follow because it is of interest to extend the heat transfer and friction factor data at other conditions than those included in the present computations. Based on the principle of similarity theory, the present data can be extrapolated or interpolated to other conditions by established correlations. For this reason, it is useful to try to obtain suitable correlations. This is another direct motivation of the present study. A question may arise whether or not correlations already exist that can predict the performance of the present heat exchanger. According to the authors' knowledge, no suitable correlations can be applied in such heat exchangers with the tube diameter around 18 mm and the number of tube-rows being larger than six. The most accurate and reliable correlations, developed by Wang et al. [8-11], with wide validation ranges is known to the present authors. However, it is again noted that the valid range for the tube diameter is between 6.35 mm and 12.7 mm, which is much smaller than that of the present model (D_o=18 mm).

The forms for correlations may be diversified, however, in order to reduce the difficulty involved in correlating the data and to refer to previous forms, the following forms are assumed.

$$f = C_1 \mathrm{Re}^{C_2} (N \cdot \frac{F_p}{D_o})^{C_3} (\frac{P_t}{P_l})^{C_4} \tag{26}$$

$$Nu = C_1 \mathrm{Re}^{C_2} (N \cdot \frac{F_p}{D_o})^{C_3} (\frac{P_t}{P_l})^{C_4} \tag{27}$$

The four coefficients C_1, C_2, C_3, C_4 should be determined by means of multiple regression technique rather than log-linear regression, which can be used to correlate a very simple form like logNu=C_1+C_2*logRe. The brief idea of multiple regression is described as follows.

6.2 Brief description of multiple regression

Consider a variable y which is related to the decision variables x_1, x_2,…, x_{M-1}, x_M. The data, obtained by computations or measurements are as presented as follows.

$$(x_{t,1}, x_{t,2}, x_{t,3}, ..., x_{t,M-2}, x_{t,M-1}, x_{t,M} \ ; \ y_t) \ , \quad t = 1, 2, ..., Nd-1, Nd$$

Assume that the form of regression equations is

$$\hat{y}_t = b_0 + b_1 x_1 + \cdots + b_{M-1} x_{M-1} + b_M x_M \tag{28}$$

It should be noted that the form of Eqs. (26) and (27) can be transformed into the form of Eq. (28) by adopting the logarithm on the two sides of these equations with $x_1 = \mathrm{Re}, x_2 = N \cdot \frac{F_p}{D_o}, x_3 = \frac{P_t}{P_l}$.

Thus the residual error is

$$EQ = \sum_{t=1}^{N} (y_t - \hat{y}_t)^2 \tag{29}$$

By using the least square theorem and the extremum theorem to find the minimum of EQ, the following equations yield

$$\frac{\partial EQ}{\partial b_0} = \frac{\partial EQ}{\partial b_1} = \cdots = \frac{\partial EQ}{\partial b_{M-1}} = \frac{\partial EQ}{\partial b_M} = 0 \tag{30}$$

The above equation can be organized as

$$(\vec{X}^T \vec{X})\ \vec{b} = \vec{X}^T \vec{Y} \tag{31}$$

where $\vec{Y} = \begin{pmatrix} y_1 \\ y_1 \\ \vdots \\ y_{Nd} \end{pmatrix}, \vec{X} = \begin{pmatrix} 1 & x_{11} & x_{12} & \cdots & x_{1M} \\ 1 & x_{21} & x_{22} & \cdots & x_{2M} \\ \vdots & \vdots & \vdots & \vdots & \vdots \\ 1 & x_{Nd1} & x_{Nd2} & \cdots & x_{NdM} \end{pmatrix}, \vec{b} = \begin{pmatrix} b_1 \\ b_1 \\ \vdots \\ b_{Nd} \end{pmatrix}$.

Denoting $A = (\vec{X}^T \vec{X})$, $B = \vec{X}^T \vec{Y}, C = A^{-1}$, Eq. (31) can be written as

$$A\vec{b} = B \quad ==> \quad \vec{b} = CB = A^{-1}B \tag{32}$$

Finally, by solving the above equation, Eq. (32), the coefficients b_0, b_1, .. , b_M can be obtained.

6.3 Multiple correlations

For the assumed form of the heat transfer and friction factor correlations, there are three decision variables, $x_1 = \mathrm{Re}, x_2 = N \cdot \frac{F_p}{D_o}, x_3 = \frac{P_t}{P_l}$, and four coefficients to be determined: $b_1 = \log C_1, b_2 = \log C_2, b_3 = \log C_3, b_4 = \log C_4$. Having introduced the idea of multiple regression, Eq. (32) is then solved by encoding the program in FORTRAN, based on the foregoing numerical data. After solving the equation, the four coefficients are determined as follows.

C_1=20.713；C_2=-0.3489；C_3=-0.1676；C_4=0.6562

The correlation for the friction factor becomes：

$$f = 20.713\,\mathrm{Re}^{-0.3489} (N \cdot \frac{F_p}{D_o})^{-0.1676} (\frac{P_t}{P_l})^{0.6265} \tag{33}$$

By using the correlation, the predicted results and original data are compared as shown in Fig. 16(a). 85% of the deviations are within 10%, and the average deviation is around 6.5%, indicating that the correlation is of sufficient accuracy.

A similar treatment for solving the transformed form of Eq. (27), gives the corresponding four coefficients as follows.

$$C_1=1.565;\ C_2=0.3414;\ C_3=-0.165;\ C_4=0.0558$$

The correlation for the Nusselt number is then written as:

$$Nu = 1.565\,\mathrm{Re}^{0.3414}\left(N\cdot\frac{F_p}{D_o}\right)^{-0..165}\left(\frac{P_t}{P_l}\right)^{0.0558} \tag{34}$$

The predicted results and numerical data are compared as shown in Fig. 16(b). All deviations are within 10%, and the average deviation is around 3.7%, indicating that the heat transfer correlation is of sufficient accuracy. Thus the heat transfer and fluid flow correlations are established as the forms of Eq.(33) and Eq.(34), and here it should be organized again that the application ranges of the present correaltions are listed as follows:

$$V_{fr} = 0.67 \sim 4.0\ \mathrm{m/s},\ \mathrm{Re} = 1000 \sim 6000,\ D_o = 16 \sim 20\ \mathrm{mm}$$
$$Fp = 2 \sim 4\ \mathrm{mm},\ P_t = 38 \sim 46\ \mathrm{mm},\ P_l = 32 \sim 36\ \mathrm{mm}$$

Returning back to the analysis of applying the correlations by Wang et al. [8-11], a comparison of the results are now shown in Fig. 17. Clearly, the predicted results by such correlations are far from the present computations. This is maybe because the established correlations have some certain application ranges, and the present geometerical parameters, e.g., the tube diameter and tube longtitudinal pitch are 18 mm

and 34 mm, respectively, are beyond the bounding values of 12.7 mm and 32 mm, respectively. Although the correlations developed by Wang et al. are so-far of much accurcy, the prediced results by those correlations are not valid for design the present heat exchangers. At this point, it is essential and necessary to develop corresponding correlations based on the numerical computations, and in turn more work such as optimization or prediction will be moved extensively forward.

7. Conclusions

In this paper, 3D-computations on air-side laminar flow and heat transfer of plain fin-and-tube heat exchangers are conducted to reveal the effects of Reynolds number, the number of tube rows, diameter of tube, fin pitch and tube pitch on the overall Nusselt number and friction factor. Also the effect of the fin surface material is observed. Based on the numerical results, the heat transfer and flow friction correlations are established. The major findings are summarized as follows.

(1). The Nusselt number and friction factor decrease with the increase of the number of tube rows, and the laminar flow and heat transfer are fully developed when the number of tube rows is larger than six.

(2). An increase of tube diameter or fin pitch decreases the heat transfer and pressure drop. The effects of tube pitch are relatively smaller than that of tube diameter and fin pitch.

(3). The heat transfer for a fin surface material with a large thermal conductivity

can be enhanced due to the decrease of the thermal resistance. The operational air velocity has also a significant effect.

(4). Due to the lack of suitable correlations applicable for the present heat exchanger, multiple correlations of the Nusselt number and friction factor have been established.

Acknowledgments

This work is supported by National Nature Science Foundation of China (No.50521604) and Program for New Century Excellent Talents in University (No. NCET-04-0938).

References

[1]. F.C.McQuiston, D.R.Tree, Heat transfer and flow friction data for two fin-tube surfaces, *ASME J. Heat Transfer,* 93(1971) 249-250.

[2]. D.G.Rich, The effect of fin spacing on the heat transfer and friction performance of multi-row, smooth plate fin-and-tube heat exchangers, *ASHRAE Transaction*, , 79(1973) 135-145.

[3]. D.G.Rich, The effect of the number of tubes rows on heat transfer performance of smooth plate fin-and-tube heat exchangers, *ASHRAE Transaction,* 81(1975) 307-317.

[4]. F.C.McQuiston, Heat mass and momentum transfer data for five plate-fin-tube heat transfer surfaces, *ASHRAE Transaction*, Part 1, 84(1978) 266-293.

[5]. F.C.McQuiston, Correlation of heat mass and momentum transport coefficients for plate-fin-tube heat transfer surfaces with staggered tubes, *ASHRAE Transaction*,

Part 1, 84(1978) 294-308.

[6]. D.L.Gray, and R.L.Webb, Heat transfer and friction correlations for plate fin-and-tube heat exchangers having plain fins, *Proc. 8th International Heat Transfer Conference*, San Francisco, California, vol. 6, pp. 2745-2750, 1986.

[7]. H.J.Kang, W.Li, H.J.Li, R.C.Xin, and W.Q.Tao, Experimental Study on Heat Transfer and Pressure Drop Characteristics of Four Types of Plate Fin-and-Tube Heat Exchanger Surfaces, *J. Thermal Science*, 3(1994) 34–42.

[8]. C.C.Wang, and K.Y.Chi, Heat transfer and friction characteristics of plate fin-and-tube heat exchangers, part I: new experimental data, *Int. J. Heat Mass Transfer*, 43(2000) 2681-2691.

[9]. C.C.Wang, K.Y.Chi, and C.J.Chang, Heat transfer and friction characteristics of plate fin-and-tube heat exchangers, part II: Correlation, *Int. J. Heat Mass Transfer*, 43(2000) 2693-2700.

[10]. C.C.Wang, Recent Progress on the Air-Side Performance of Fin-and-Tube Heat Exchangers, *Int. J. Heat Exchangers*, 2(2000) 57-84.

[11]. C.C.Wang, Heat Exchanger Design, Taiwan: Wunan Press, China, 2003. (In Chinese)

[12]. A.Bestani, N.K.Mitra, and M.Fiebig, Numerical simulation of flow field in a fin tube heat exchanger, *ASME J. Fluids Engineering*, 101(1990) 91-96.

[13]. K.Torikoshi, G.Xi, Y.Nakazama, and H.Asano, Flow and heat transfer performance of a plate-fin and tube heat exchanger, *Heat Transfer*, 4(1994) 411-416.

[14]. J.Y.Jang, M.C.Wu, and W.J.Chang, Numerical and experimental studies of three-dimensional plate-fin and tube heat exchangers, *lnt. J. Heat Mass Transfer,* 39(1996) 3057-3066.

[15]. J.Y.Jang, and J.Y.Yang, Experimental and 3-D numerical analysis of the thermal-hydraulic characteristics of elliptic finned-tube heat exchangers, *Heat Transfer Engineering*, 19(1998) 55-67.

[16]. Y. L.He, W.Q.Tao, F.Q.Song, and W.Zhang, Three-dimensional numerical study of

heat transfer characteristics of plain plate fin-and-tube heat exchangers from view point of field synergy principle, *Int. J. Heat Fluid Flow*, 6(2005) 459-473.

[17]. A.Erek, B.Ozerdem, and L.Bilir, Effect of geometrical parameters on heat transfer and pressure drop characteristics of plate fin and tube heat exchangers, *Applied Thermal Engineering,* 25(2005) 2421-2431.

[18]. G.N.Xie., Improvements of fin-and-tube heat exchangers and their Design Optimizations, Ph.D. Thesis, School of Energy and Power Engineering, Xi'an Jiaotong University, 2007. (In Chinese)

[19]. L.H.Tang, M.Zeng, G.N.Xie, and Q.W.Wang, Fin pattern effects on air-side heat transfer and friction characteristics of fin-and-tube heat exchangers with large number of large-diameter tube rows, *Heat Transfer Engineering*, *accepted, 2007*.

[20]. L.H.Tang, G.N.Xie, M.Zeng, H.G.Wang, X.H.Yan, and Q.W.Wang, Experimental investigation on heat transfer and flow friction characteristics in three types of plate fin-and-tube heat exchangers, *Journal of Xi'an Jiaotong University*, 41(2007): 521-525. (In Chinese)

[21]. G.N.Xie, Q.W.Wang, and B.Sunden, Application of a genetic algorithm for thermal design of fin-and-tube heat exchangers, *Heat Transfer Engineering*, *accepted, in press, 2007.*

[22]. G.N.Xie, B.Sunden, and Q.W.Wang, Optimization of Compact Heat Exchangers by a Genetic Algorithm，Applied Thermal Engineering，*accepted, in press, 2007.*

[23]. G.N.Xie, Q.Y.Chen, M.Zeng, and Q.W.Wang, Thermal design of heat exchangers with fins inside and outside of tubes, *Proceedings of GT2006, ASME Turbo Expo 2006*, May 8-11, 2006, Barcelona, Spain. Paper.no GT2006-90260.

[24]. G.N.Xie, Q.W.Wang, and M.Zeng, Genetic algorithm based design and optimization of outer-fins and inner-fins tube heat exchangers, *Proceedings of GT2007, ASME Turbo Expo 2007*, May 14-17, 2007, Montreal, Canada. Paper.no GT2007-27889.

[25]. G.N.Xie, Q.W.Wang, M.Zeng, and L.Q.Luo, Heat transfer analysis for

shell-and-tube heat exchangers with experimental data by artificial neural networks approach, *Applied Thermal Engineering*, 27(2007) 1096-1104.

[26]. Q.W.Wang, G.N.Xie, M.Zeng, and L.Q.Luo, Prediction of heat transfer rates for shell-and-tube heat exchangers by artificial neural network approach, *Journal of Thermal Science,* 15(2006) 257-262.

[27]. W.Q.Tao, Numerical Heat Transfer, 2d ed., **Xi'an** Jiaotong University Press, Xi' an, China, 2001. **(In Chinese)**

[28]. Y.P.Cheng，Z.G.Qu，and W.Q.Tao, Numerical design of efficient slotted fin surface based on the field synergy principle, *Numerical Heat Transfer, Part A*, 45(2004) 517-538.

[29]. Z.G.Qu, W.Q.Tao, and Y.L.He, 3D numerical simulation on laminar heat transfer and fluid flow characteristics of strip fin surface with X-arrangement of strip, *ASME J. Heat Transfer*, 126(2004) 69-707.

[30]. J.J.Zhou, and W.Q.Tao, Three dimensional numerical simulation and analysis of the airside performance of slotted fin surfaces with radial strips, *Engineering Computations*, 22(2005) 940-957.

[31]. W.Q.Tao, W.W.Jin, Y.L.He, Z.G.Qu, and C.C.Zhang, Optimum design of two-row slotted fin surface with x-shape strip arrangement positioned by ''front coarse and rear dense'' principle, Part I: physical/mathematical models and numerical methods. *Numerical Heat Transfer, Part A*, 50(2006) 731-749.

[32]. W.W.Jin, Y.L.He, Z.G.Qu, and W.Q.Tao, Optimum design of two-row slotted fin surface with x-shape strip arrangement positioned by "front coarse and rear dense"' principle, Part II: results and discussion. *Numerical Heat Transfer, Part A* , 50(2006) 751-771.

[33]. S.V.Patankar, Numerical Heat Transfer and Fluid Flow, McGraw-Hill, New York, 1980.

[34]. T.E.Schmidt, Heat transfer calculations for extended surfaces, *Refrigerating Engineering*, 57(1949) 351-357.

[35]. L.H.Tang, G.N.Xie, M.Zeng, Q.W.Wang, Numerical simulation of fin patterns on air-side heat transfer and flow friction characteristics of fin-and-tube heat exchangers, Proceedings of ASCHT07, *1st Asian Symposium on Computational Heat Transfer and Fluid Flow*, October 18-21, 2007, Xi'an, China.

Figure Captions

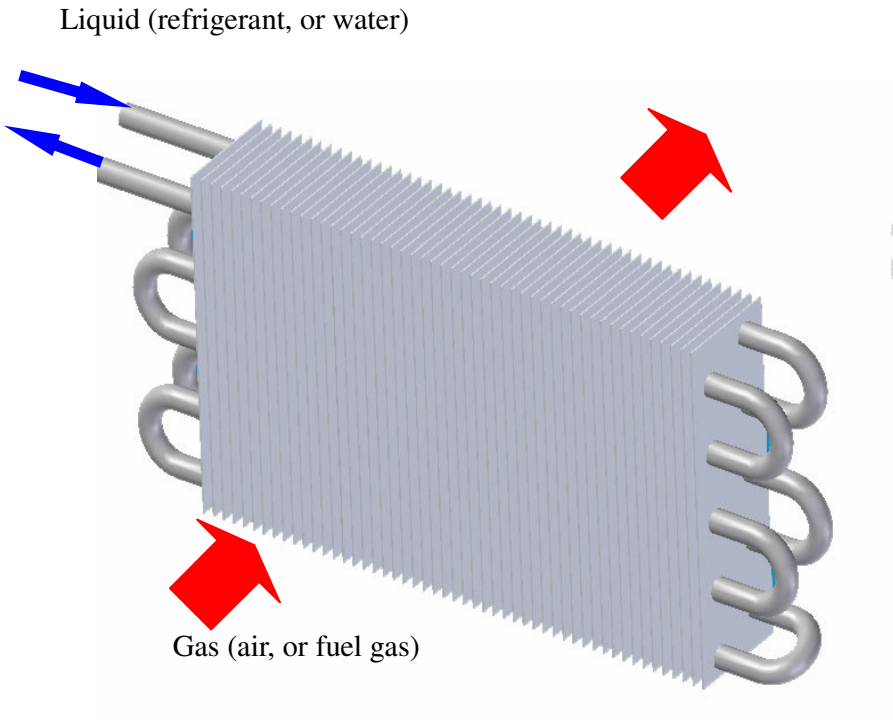

Fig.1 A typical fin-and-tube heat exchanger

(The gas**,** such as air or fuel gas, needs to be cooled, flows normal to the finned bundle and the cooling liquid, such as a refrigerant or water, flows through the tubes. Industrial applications are, e.g., air-coolers, fan coils, heaters, and inter- coolers, etc.)

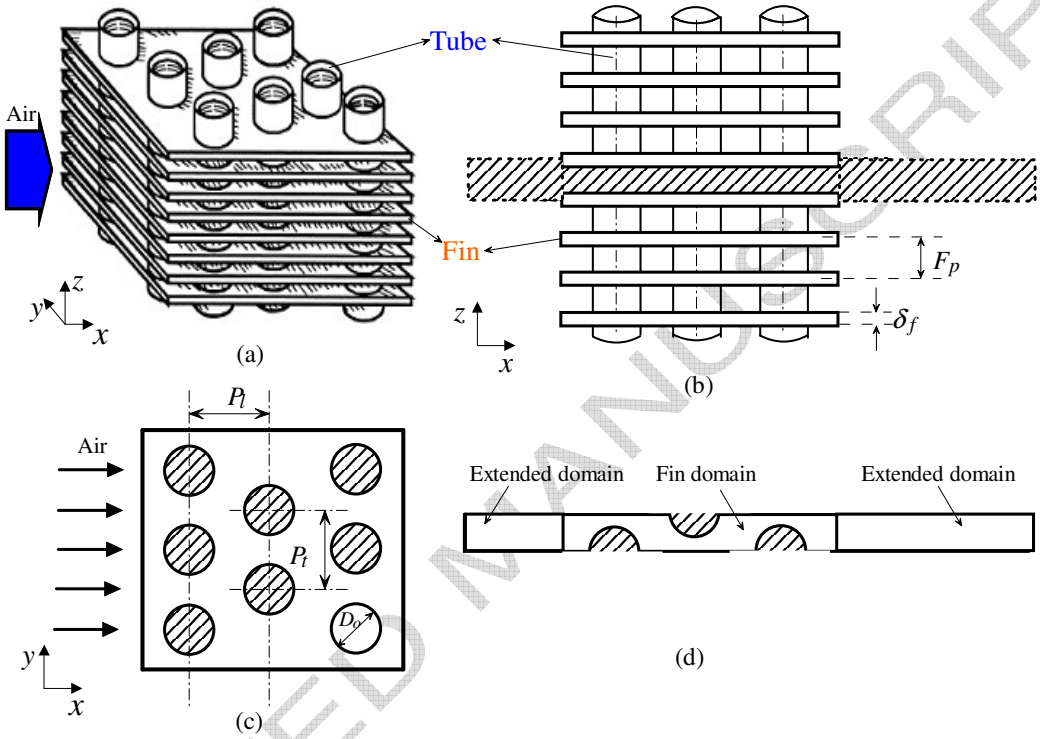

Fig. 2 Schematic configuration of a heat exchanger
(for saving space, a configuration of three tube-rows is shown, not the fixed geometry for all computations in this study)

(a) The overall core: air flows across the finned bundle.

(b) Cross-section in z-x plane: computational domain is selected as the space between two adjacent fin surfaces and the shaded extended regions bounded by dashed lines.

(c) Cross-section in y-x plane: the tubes are in staggered arrangement.

(d) Cross-section of computational domain in y-x plane: extensions at entrance 1.5 fin length, at exit 5 fin lengths, respectively.

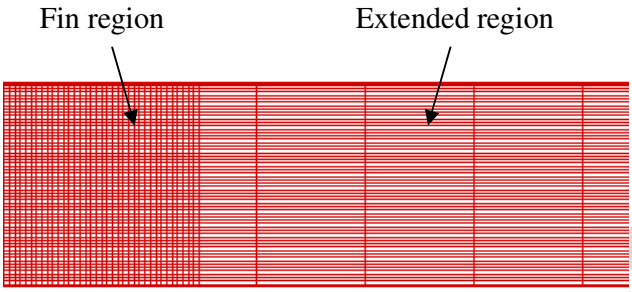

(a) Grid distribution: the grid space in the fin region is 20 times denser than that of the extended region

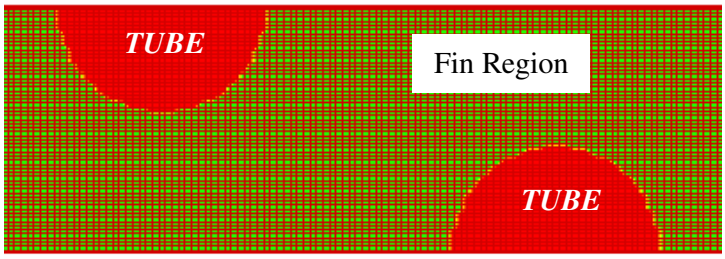

(b) Grid in fin region: circle bound is well approximated by step-wise bound due to the fine grid

Fig. 3 Non-uniform grids for computations

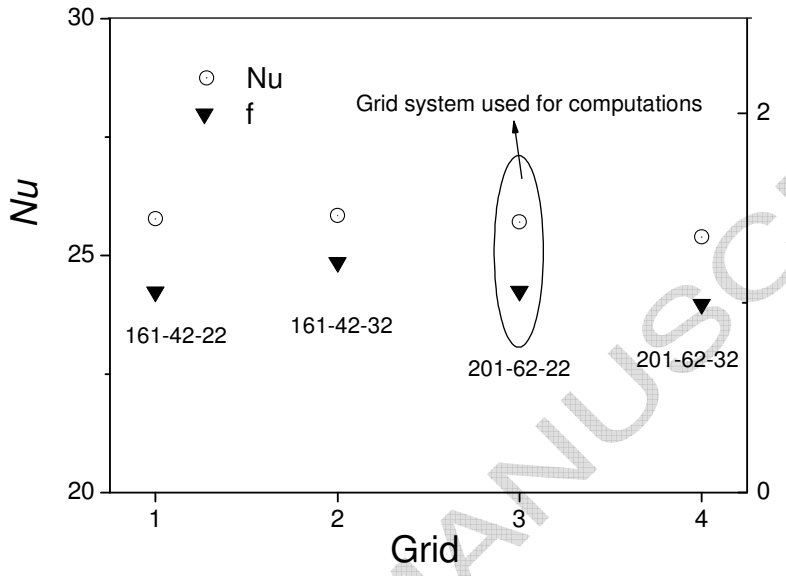

Fig. 4 The results of grid independence tests: the grid system 201-62-22 is used for all computations

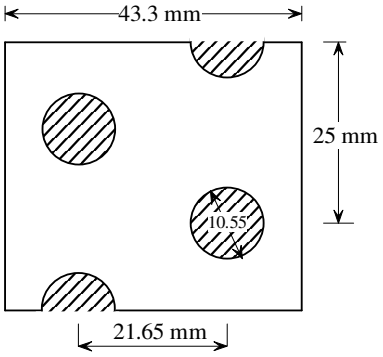

(a) Schematic configuration of the test case: a heat exchanger having two tube-rows

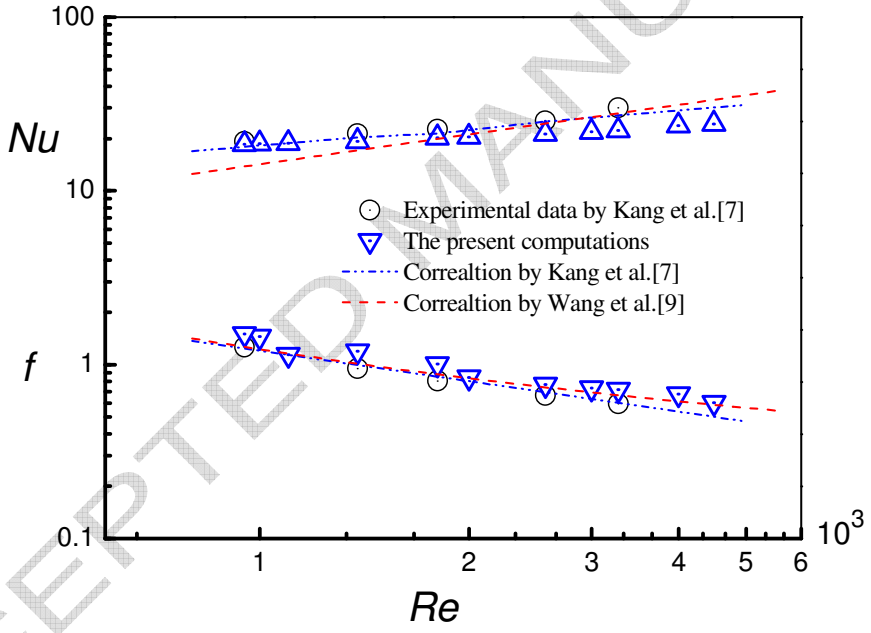

(b) Comparison of Nusselt number and friction factor

Fig. 5 Validation of the model and code with a test case

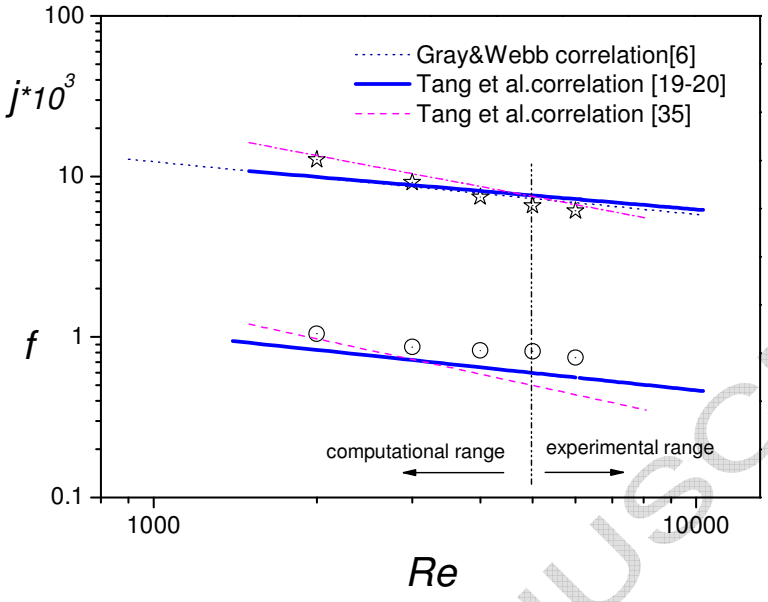

Fig. 6 Comparison between the present laminar model and correlations

(Gray and Webb correlation [6]: $500 \le \mathrm{Re} \le 24700,\ N = 4$

Tang et al. correlation [19-20,35]: $4000 \le \mathrm{Re} \le 10000,\ N = 6$ **)**

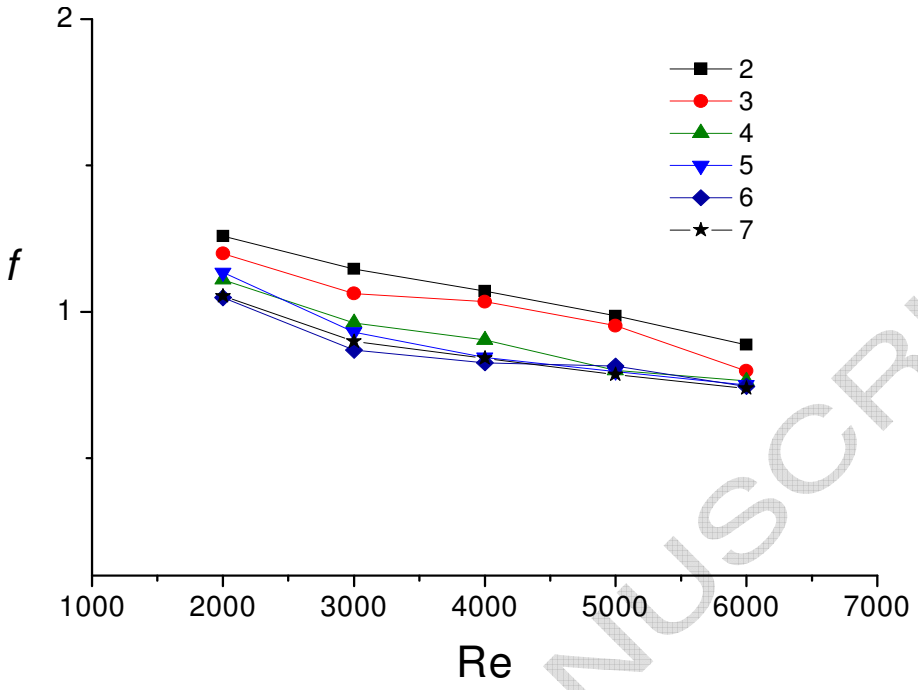

(a) Friction factor

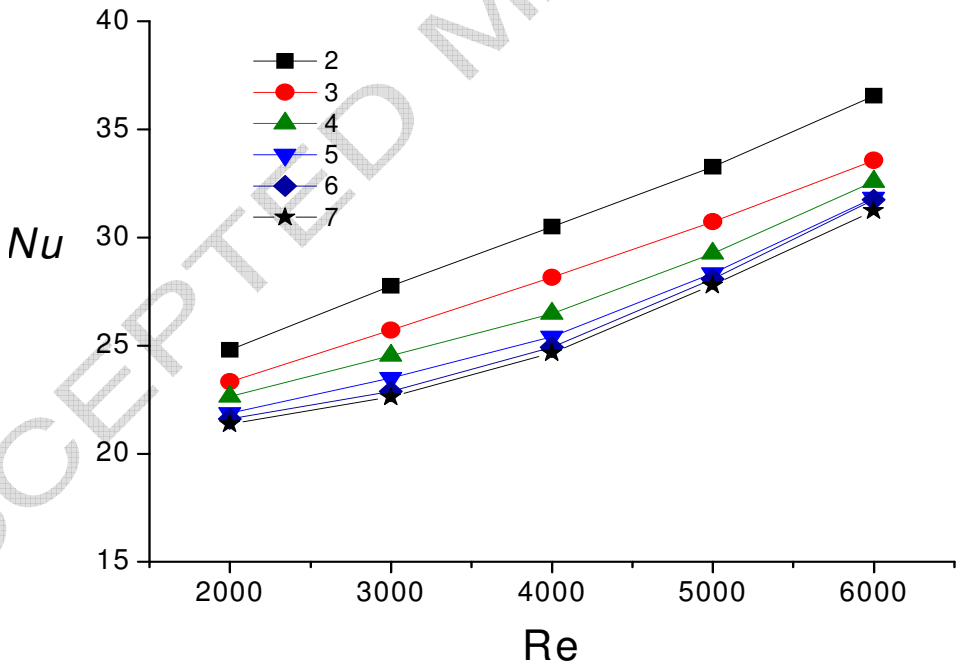

(b) Nusselt number

Fig. 7 The effects of Reynolds number and the number of tube rows on Nusselt number and friction factor

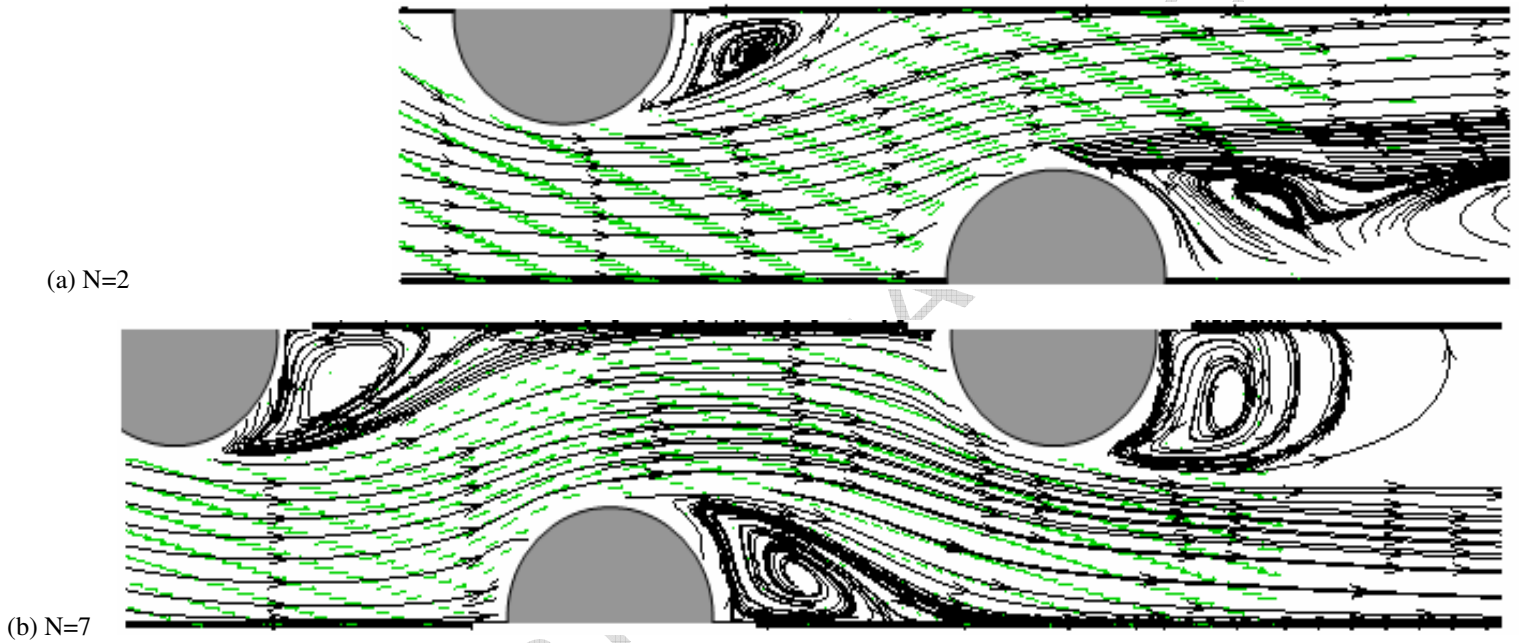

(a) N=2

(b) N=7

Fig. 8 Streamlines for two-rows and seven-rows (Re=3000): x-y plane at Z=0.015mm.
(a) N=2: display of overall fin region ; (b) N=7: display of the last three-rows in fin region

(a) N=2

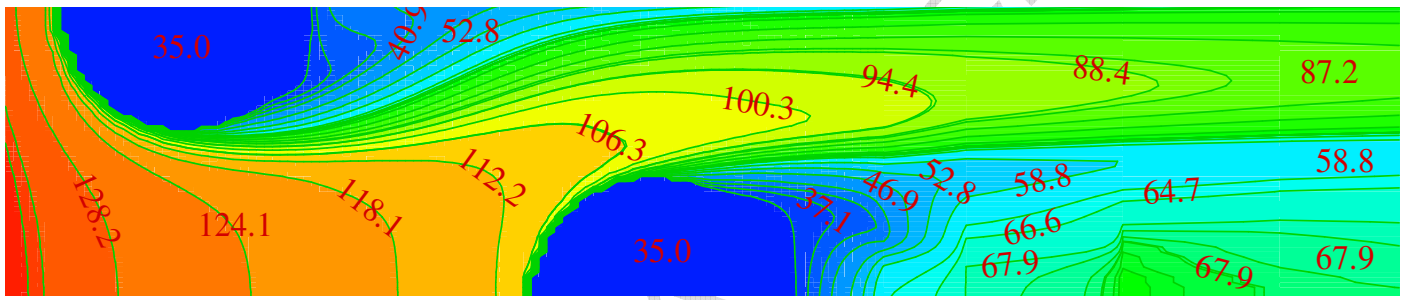

(b)N=7

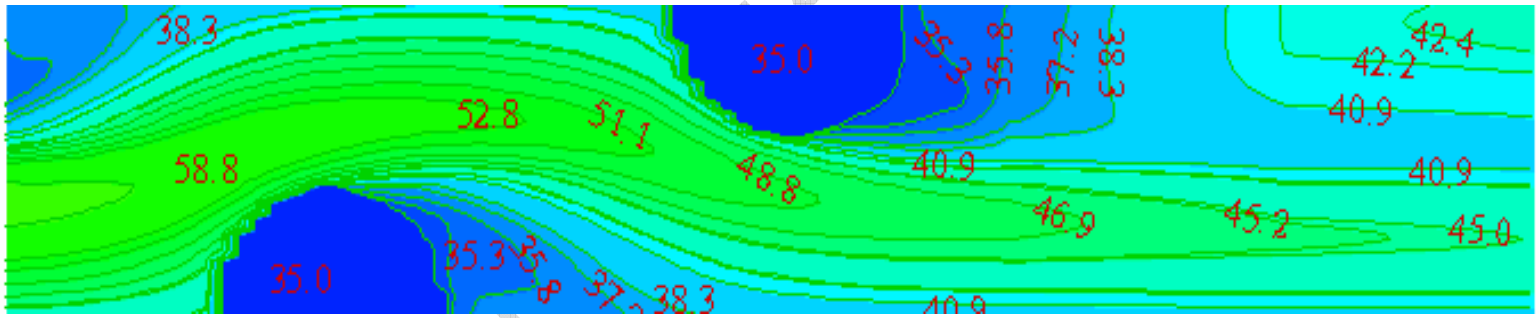

Fig. 9 Isotherms for two-rows and seven-rows (Re=3000)
(a) N=2: display of overall fin region ; (b) N=7: display of the last three-rows in fin region

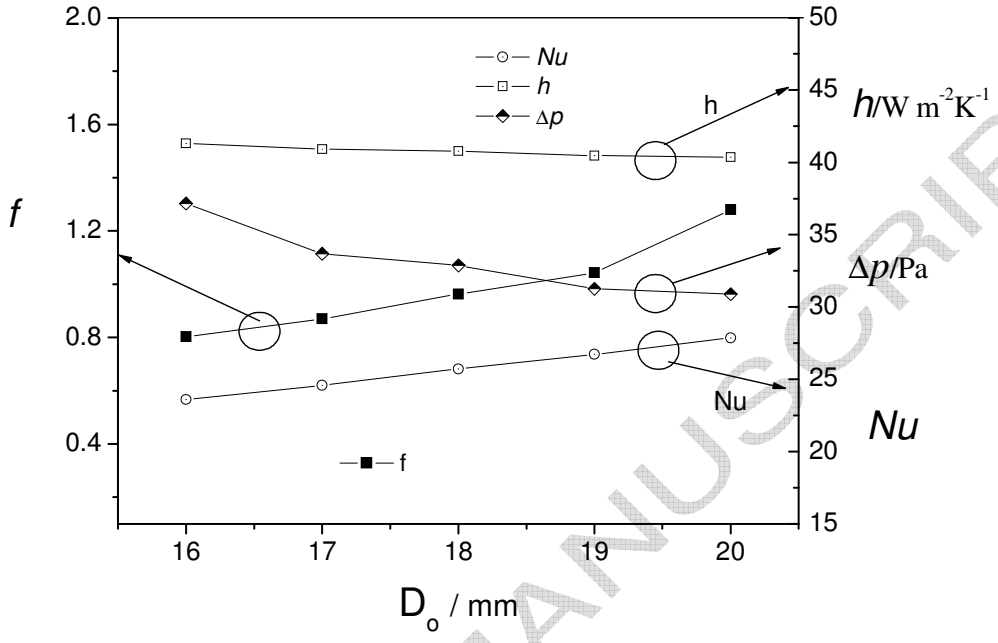

Fig. 10 The effects of tube diameter on Nusselt number, friction factor, heat transfer coefficient and pressure drop (N=3, Re=3000)

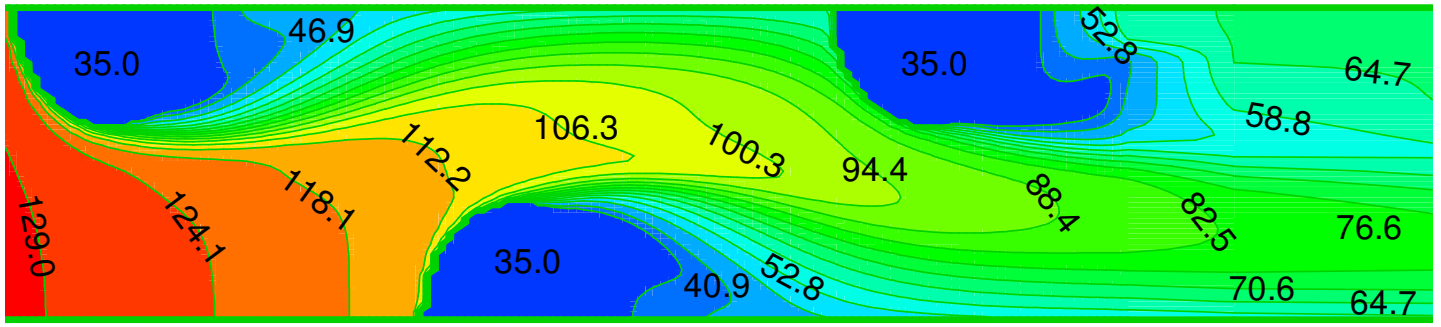

(a) D=-16mm

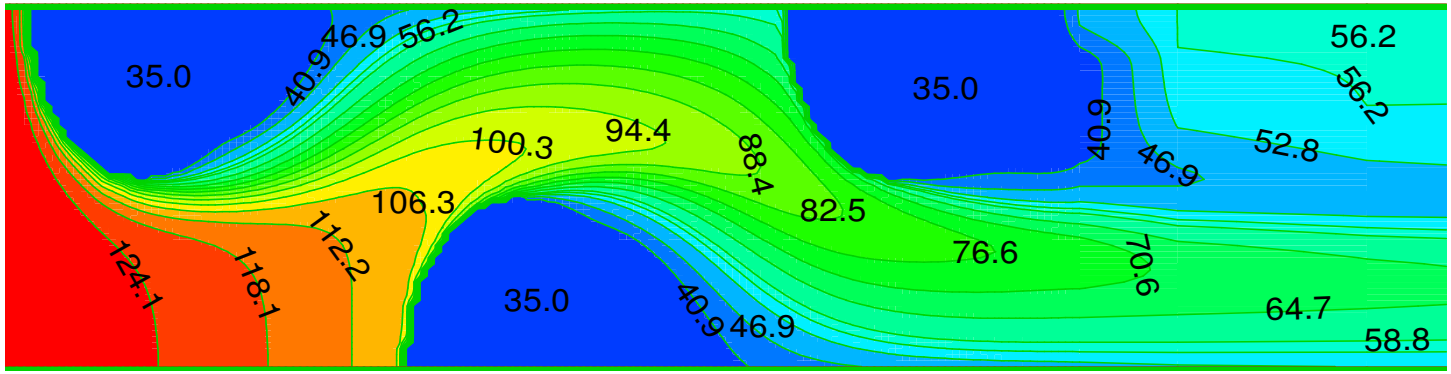

(b) D=20mm

Fig. 11 Isotherms for D=16mm and D=20mm (Re=3000, N=3)

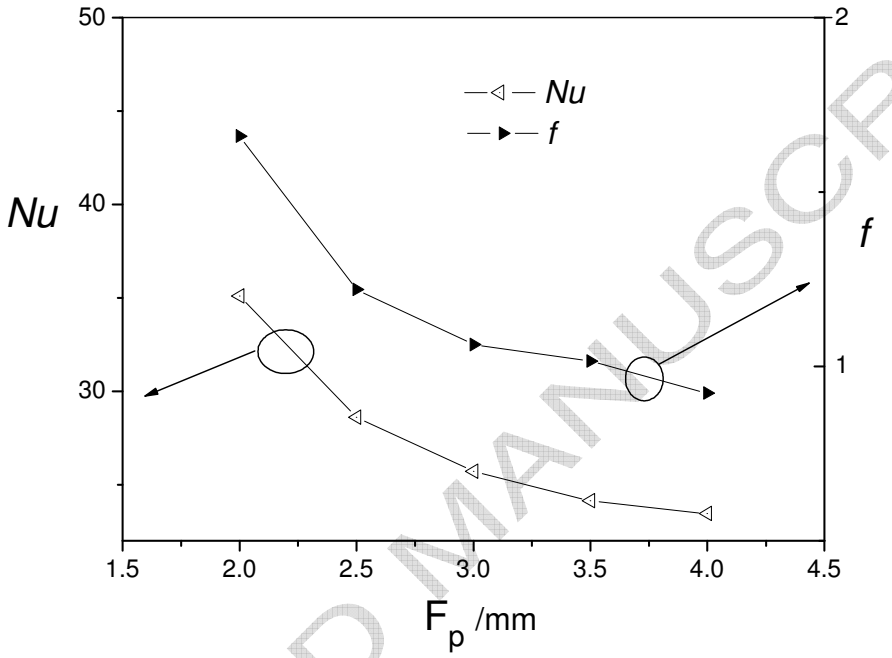

Fig. 12 The effects of fin pitch on Nusselt number and friction factor (N=3, Re=3000)

(a) Fs=2 mm

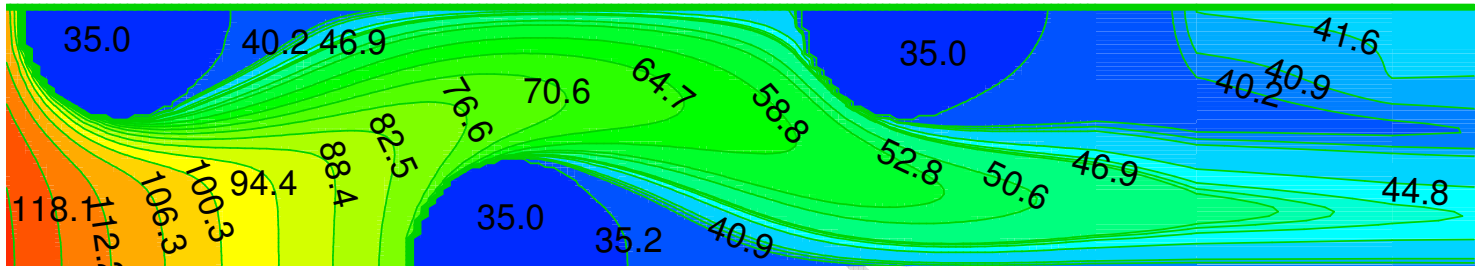

(b) Fs=4 mm

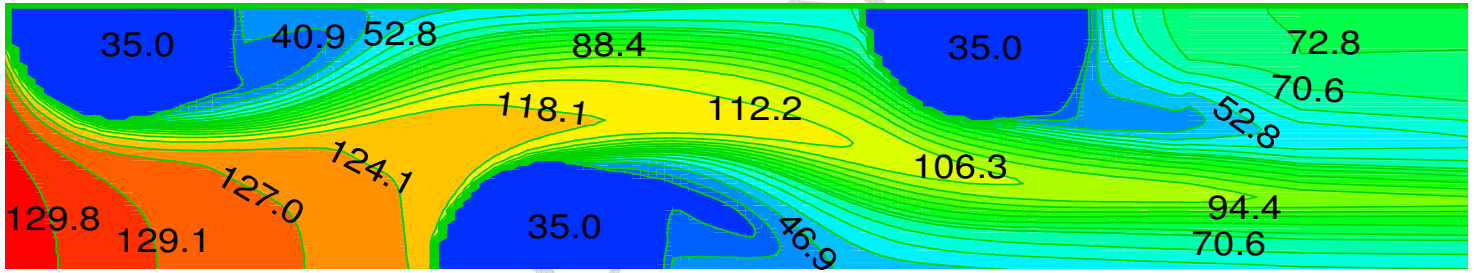

Fig. 13 Isotherms for F_p=2 mm and F_p=4 mm (Re=3000, N=3)

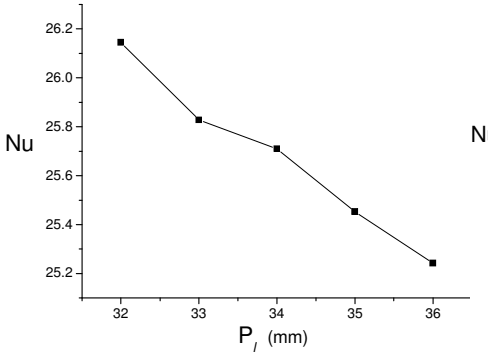

(a) Nusselt number: Longitudinal pitch

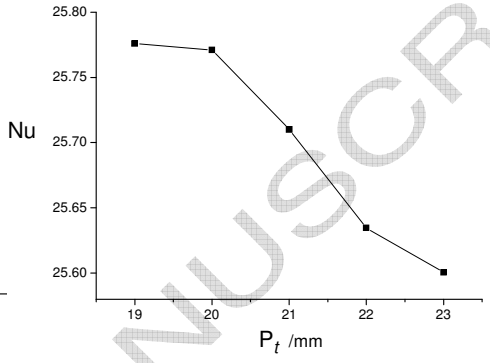

(b) Nusselt number: Transverse pitch

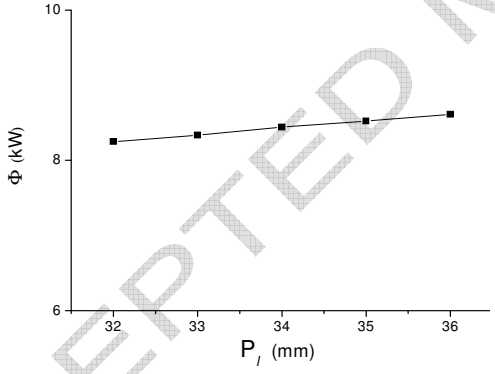

(c) Heat transfer rate: Longitudinal pitch

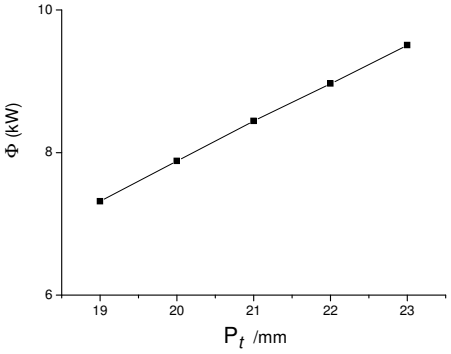

(d) Heat transfer rate: Transverse pitch

Fig. 14 The effects of tube pitch on Nusselt number (N=3, Re=3000)

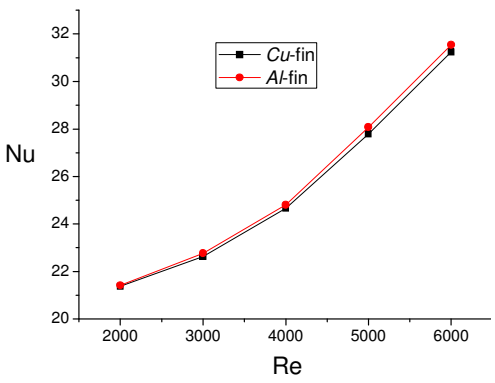

(a) Nusselt number
(The fin efficiency has been separated)

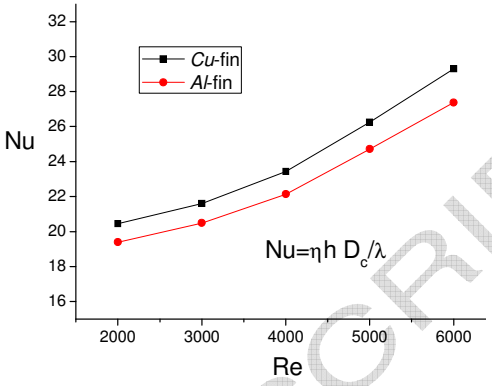

(b) Nusselt number
(The fin efficiency has been included)

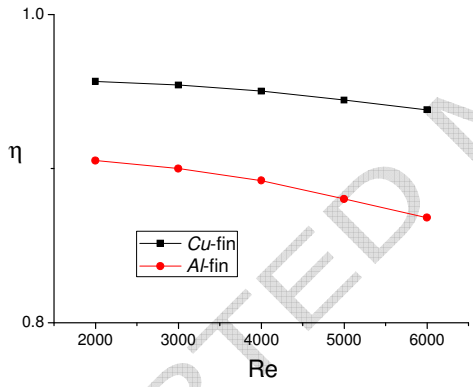

(c) Fin efficiency

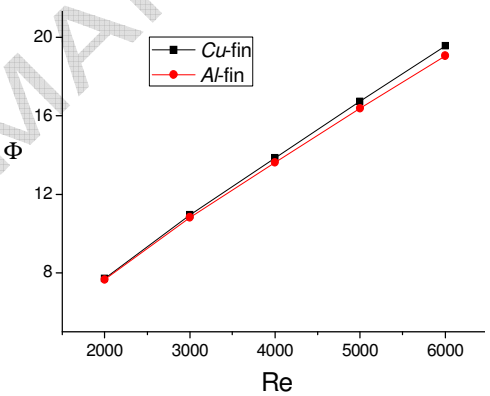

(b) Heat transfer rate

Fig. 15 The effects of fin surface material on Nusselt number, fin efficiency and heat transfer rate (N=7)

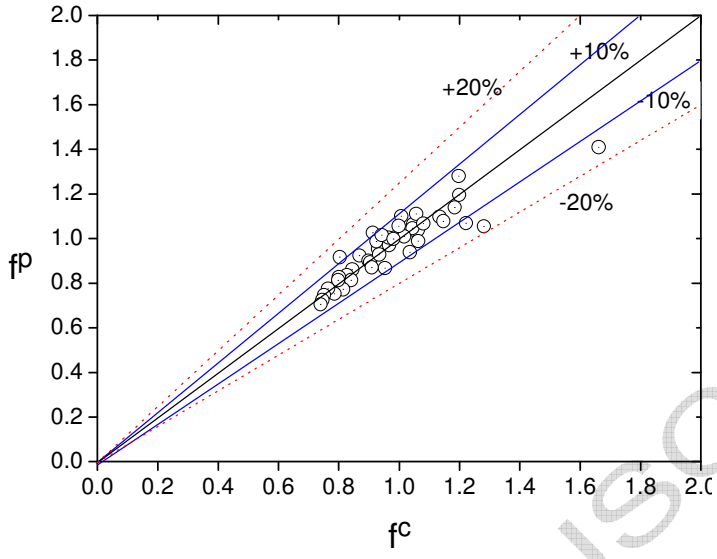

(a) friction factor

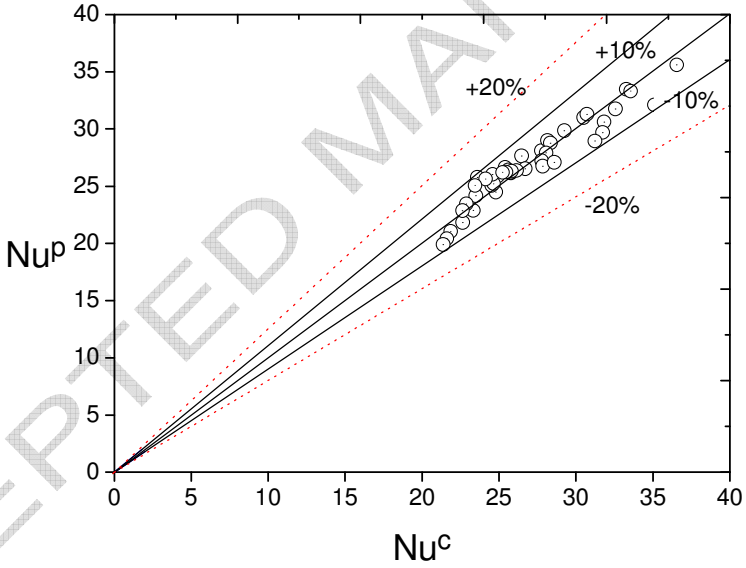

(b) Nusselt number

Fig. 16 Comparison between predicted results and numerical data: the variable in the x-coordinate refers to the numerical data through computations, while the variable in the y-coordinate stands for the prediction through the multiple correlations

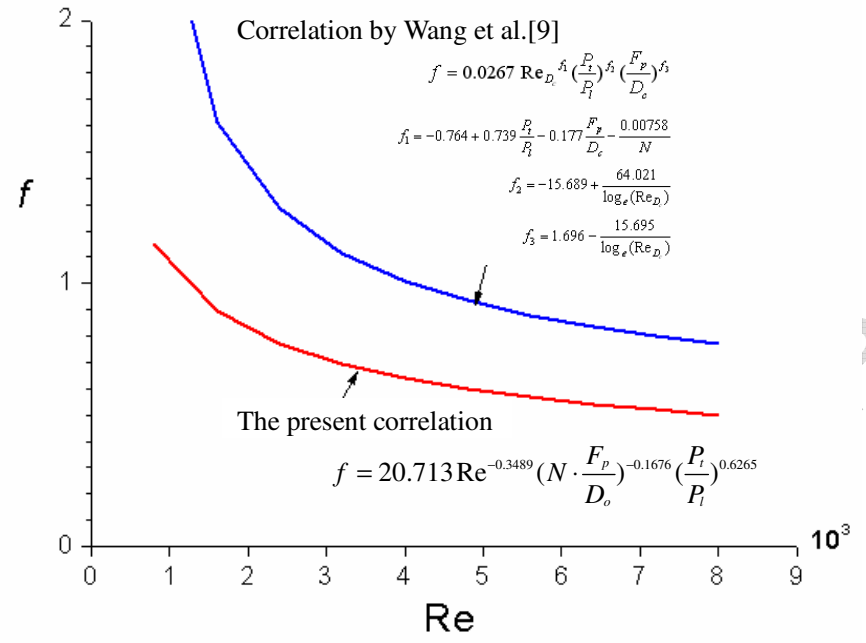

(a) Friction factor

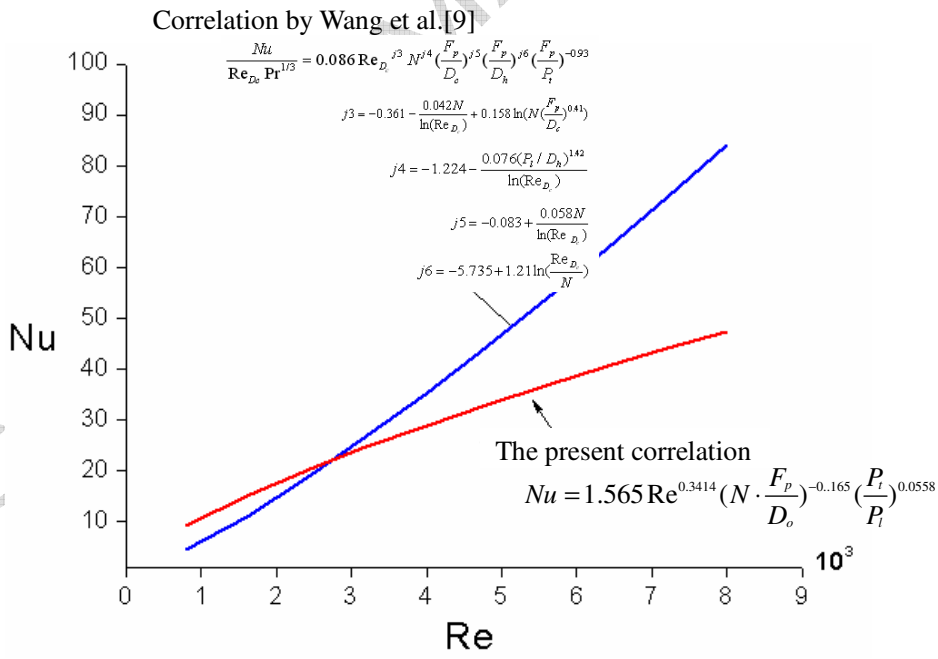

(b) Nusselt number

Fig. 17 Comparison of results predicted from correlations by Wang et al. [9] and the present correlations: The large deviation of Wang's correlations indicates that these correlations are not suitable**.**